Journal of Materials Science & Technology 62 (2021) 254–267

Contents lists available at ScienceDirect

Journal of Materials Science & Technology

journal homepage: www.jmst.org

Invited Review

Review on modelling of corrosion under droplet electrolyte for predicting atmospheric corrosion rate

Bangalore Gangadharacharya Koushik[a,*], Nils Van den Steen[a], Mesfin Haile Mamme[a,b], Yves Van Ingelgem[a], Herman Terryn[a,*]

[a] Vrije Universiteit Brussel, Research Group Electrochemical and Surface Engineering (SURF), Pleinlaan 2, 1050 Brussels, Belgium
[b] Vrije Universiteit Brussel, Eenheid Algemene Chemie (ALGC), Pleinlaan 2, 1050 Brussels, Belgium

ARTICLE INFO

Article history:
Received 21 February 2020
Received in revised form 18 April 2020
Accepted 30 April 2020
Available online 8 July 2020

Keywords:
Atmospheric corrosion
Water droplets
Mathematical modelling
Condensation
Evaporation

ABSTRACT

Atmospheric corrosion of metals is the most common type of corrosion which has a significant impact on the environment and operational safety in various situations of everyday life. Some of the common examples can be observed in land, water and air transportation systems, electronic circuit boards, urban and offshore infrastructures. The dew drops formed on metal surface due to condensation of atmospheric moisture facilitates corrosion as an electrolyte. The corrosion mechanisms under these droplets are different from classically known bulk electrolyte corrosion. Due to thin and non-uniform geometric thickness of the droplet electrolyte, the atmospheric oxygen requires a shorter diffusion path to reach the metal surface. The corrosion under a droplet is driven by the depletion of oxygen in the center of the droplet compared to the edge, known as differential aeration. In case of a larger droplet, differential aeration leads to preferential cathodic activity at the edge and is controlled by the droplet geometry. Whereas, for a smaller droplet, the oxygen concentration remains uniform and hence cathodic activity is not controlled by droplet geometry. The geometry of condensed droplets varies dynamically with changing environmental parameters, influencing corrosion mechanisms as the droplets evolve in size. In this review, various modelling approaches used to simulate the corrosion under droplet electrolytes are presented. In the efforts of developing a comprehensive model to estimate corrosion rates, it has been noted from this review that the influence of geometric evolution of the droplet due to condensation/evaporation processes on corrosion mechanisms are yet to be modelled. Dynamically varying external factors like environmental temperature, relative humidity, presence of hygroscopic salts and pollutants influence the evolution of droplet electrolyte, making it a complex phenomenon to investigate. Therefore, an overview of available dropwise condensation and evaporation models which describes the formation and the evolution of droplet geometry are also presented from an atmospheric corrosion viewpoint.

Contents

* Corresponding authors.
E-mail addresses: kbangalo@vub.be (B.G. Koushik), herman.terryn@vub.be (H. Terryn).

https://doi.org/10.1016/j.jmst.2020.04.061
1005-0302/

Nomenclature

β_{Fe}	Tafel slope for the iron oxidation reaction
ΔT	Temperature difference between the surrounding and the surface
δ	Electrolyte thickness
γ	Fractional coverage of the corrosion products
Φ_m - Φ_0	the potential driving force
ρ	Density of condensing liquid
σ_{lv}	Surface tension
θ	Contact angle
b	Area ratio of TPB zone and electrochemical reaction zone
$C_{O_2,3B}$	Concentration of oxygen in TPB zone
$C_{O_2,bulk}$	Bulk concentration of oxygen
D	Diffusion coefficient
F	Faraday constant
g	Ratio of TPB length to the area of electrochemical reaction zone
H_{lv}	Specific enthalpy of evaporation
i_{3B}	Cathodic limiting current density in TPB zone
i_{bulk}	Cathodic limiting current density in bulk zone
i_d	Total cathodic limiting current
i_k,Fe	Kinetic current density
$i_{p,Fe}$	Passivation current density
k	Cathodic reaction rate constant
$K_{0,Fe}$	Rate constant with unit of Am mol-1
L	TPB length
n	Number of transferred electrons
R	Radius of the droplet
r_{min}	Minimum radius of the droplet
S	Area of the electrochemical reaction zone
S_{3B}	Area of TPB zone
Ts	Surface temperature
TOW	Time of wetness
TPB	Triple phase boundary

1. Introduction

Atmospheric corrosion of a metal is a spontaneous degradation process resulting from interactions with its surrounding environment [1]. Metal degradation due to atmospheric exposure has a significant impact on the society [2]. According to the recent analysis, the overall cost of corrosion is estimated to be 3.4 % of global GDP [3–5], of which, atmospheric corrosion accounts for approximately half the annual cost of all types of metal corrosion [6]. Most frequently, the atmospheric corrosion processes are initiated by wetting of metal surface by direct condensation of atmospheric moisture due to temperature changes of a clean surface, and by chemical condensation due to hygroscopic properties of surface contaminants such as salts and industrial pollutants deposited on the surface [7–11]. The complex process of condensation of atmospheric moisture due to temperature changes in combination with hygroscopic effect of surface contaminants leads to formation of droplets on the surface [12–16] and eventually a thin film of water [17,18] that facilitates corrosion by serving as the electrolyte [19,20].

Depending on the surface temperature and wettability, in combination with the environmental humidity and temperature, droplets exhibit different dimensions and population densities on the surface, resulting in different corrosion rates [21–25]. Besides the condensation of atmospheric moisture due to temperature changes and hygroscopic properties of surface contaminants, the electrolyte can also be deposited on the metal surface due to fog, rain and melting snow, which are not considered in this review [1,26–31]. Therefore, this review deals with process-based modelling of corrosion of metal under droplet electrolyte formed by direct condensation of atmospheric moisture due to surface temperature changes. Models describing the hygroscopic properties of surface contaminants that determines the duration of wetness and influences the wetting/drying cycles during atmospheric corrosion has been discussed in detail by Schindelholz et al. [32].

The corrosion mechanisms under the droplet electrolyte are different from classically known bulk electrolyte corrosion [33]. In case of bulk electrolyte, the corrosion process is often controlled by the rate of diffusion of oxygen through the electrolyte which is generally quantified as diffusion-limited cathodic current [34]. Whereas, in case of droplet electrolyte, the atmospheric oxygen diffuses through a rather very short path between the interface of air-electrolyte and the metal. Therefore, oxygen is readily available to facilitate the corrosion reactions [35]. Due to the curvature of the droplet, the shortest path for oxygen diffusion is along the outer edge of the droplet, resulting in a differential aeration electrochemical cell that drives the corrosion reactions [36]. The evolution of droplet size causes variation in radius of curvature and hence the degree of differential aeration, which in-turn influences the corrosion mechanisms [21,23–25,37–39]. The concentration of the dissolved salts in the droplet that determines the conductivity of the electrolyte is a function of droplet size [40]. As the corrosion reaction proceeds, the dilution of the corrosion products in the droplet is also controlled by the size of the droplet electrolyte. Additionally, the dimensions of a droplet electrolyte dynamically vary with multiple changing factors like environmental temperature, relative humidity, presence of hygroscopic salts [20], pollutants, surface properties of metal and precipitation of corrosion products, making it very challenging to investigate the corrosion rate by controlling the droplet dimensions.

Currently available methods to quantify the atmospheric corrosion rate, is either by accelerated corrosion tests [41–44] or by huge time-consuming field exposure experiments [45,46]. Accelerated corrosion tests do well in quantifying corrosion rate at specific conditions but do not give a general understanding because the experimental condition often does not replicate the real atmospheric environment. Therefore, significant efforts are being devoted to developing models describing all the physical and chemical processes involved in atmospheric corrosion of a metal [47,48]. The simulation models are intended to predict the corrosion rates for a given environmental condition, thus saving both time and cost involved in estimating atmospheric corrosion rates of metal.

Both analytical and numerical approaches used to model corrosion under droplet electrolyte are described in this review.

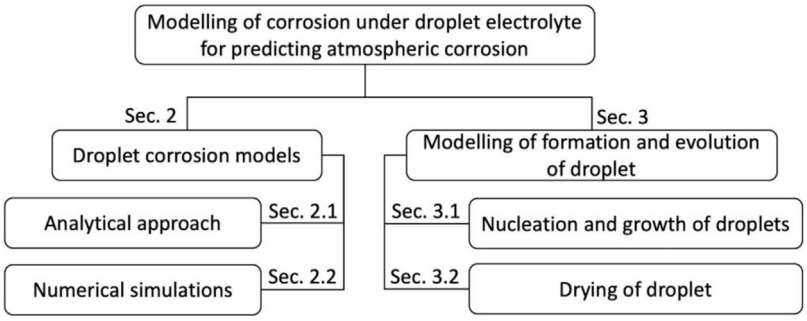

Fig. 1. Classifications of various modelling and simulation methods for droplet corrosion along with their formation and evolution.

The analytical model has focused on estimating the corrosion rates based on derived equations for cathodic limiting current [49]. Due to the inherent limitations of analytical approaches, the focuses on numerical approaches are being employed to comprehensively predict the corrosion rates and state of surfaces over a wide range of conditions. The numerical approaches accounted for aspects like oxygen diffusion, cathodic/anodic reactions, active-passive transitions and oxide layer formation. In the numerical approach, the corrosion rates are determined by solving the involved physicochemical and electrochemical equations in space and time domains. However, the consideration of formation and evolution of droplets on corroding surface is still missing in the existing models. Since the atmospheric corrosion processes are initiated only after a droplet electrolyte of certain size is residing on the surface [24] and is influenced by the geometric evolution of droplets [24]. It becomes important for the model to include the condensation processes of atmospheric moisture on the surface. After an early effort to analytically model corrosion under evaporating droplet by Lyon et al. [17], modelling the formation [50] and evolution of electrolyte due to condensation/evaporation [20,51] of atmospheric moisture for estimation of corrosion rates is recently gaining importance and awaits extensive investigation.

An ideal simulation model needs to account for the following to have a holistic droplet corrosion model. (1) Geometric size of the droplet: The open-circuit potential (OCP) was higher for the smaller droplets compared to the larger droplets [24]. The cathodic corrosion current density increased with decreasing size of NaCl droplets due to shorter diffusion path for oxygen from ambient to the corroding surface for smaller droplets [24]. (2) Surface energy: The tendency towards localized corrosion decreased in case of droplet decreasing thickness and constant area, which is attributed to more homogeneous oxygen transfer process under a thinner droplet [21]. Corrosion damage during the drying cycles appeared to be enhanced for large droplets with high contact angle and for increased electrolyte concentration. The contact angle and hence the thickness on droplets depends of the surface energy of the corroding surface [52]. The surface energy of the corroding surface is altered due to the corrosion precipitates and oxide layer formation, which is in-turn influenced by the pH [24] of the electrolyte [53].

To consider the formation and evolution of droplets on a metal surface, existing approaches to model dropwise condensation are presented in this review. Both experimental studies and mechanistic modelling of dropwise condensation phenomenon has been an important topic of research in the field of heat exchangers and refrigeration over a past few decades. This is mainly due to the enhanced heat exchange coefficient of dropwise condensation [18,54–69]. Condensation of atmospheric moisture is a nucleation phenomenon which results in a distribution of droplets on the surface [13,14,70]. In general, the complete cycle of dropwise condensation is classified into five phases: nucleation, aggregation, growth, coalescence and sliding. Sliding only occurs on an inclined surface and on a surface with differential wettability regions, and both are not relevant in case of flat surfaces with uniform wettability as addressed in this review.

There are three main sections in this paper. The first section presents the state-of-the-art of the models describing corrosion under the droplet electrolyte, highlighting the influence of droplet geometry and passivation due to corrosion precipitates, along with other relevant parameters. The second section presents an overview of the numerical models for simulating droplet condensation/evaporation process in the perspective of atmospheric corrosion by highlighting the parameters relevant for droplet corrosion modelling. Fig. 1 shows the classifications of modelling approaches described in the following sections. Finally, in the third section, discussion is made to identify the points to come to a proper understanding of the process to have a realistic model for long-term prediction of atmospheric corrosion rates.

2. Droplet corrosion models

Due to many challenges involved in modelling of localized corrosion [71], the research on modelling droplet corrosion is still in an infant stage. The available literature on modelling of droplet corrosion largely adopts a configuration similar to Evans drop experiment [72–74]. Evans placed a NaCl drop on a horizontal steel surface in contact with air and followed the development of anodic and cathodic areas under the drop using phenolphthalein and ferricyanide as indicators. The cathodic area turned red due to the presence of OH^- ions resulting from the oxygen reduction reaction (ORR) and the anode area turned blue due to the presence of Fe^{2+} ions.

It was found that the area towards the edge of the droplet had ready access to oxygen from atmospheric air and functioned as cathode. Areas under the center of the drop had less access to oxygen because the dissolved oxygen needed to diffuse through the volume of drop to reach the liquid-metal interface at the center of the drop. Thus, the area under the center of the drop functioned as an anode. These sub-processes are schematically shown in Fig. 2. The anodic area expanded outwards with time to meet the cathodic area, and rings of rust were formed at their interface. The difference in oxygen concentration between the edge and center of the droplet is known as differential aeration and is attributed to the geometry of the droplet. Hence the magnitude of differential aeration depends on the geometric size and shape of the droplet, which in-turn influences the corrosion rate [24,25]. The corrosion under a droplet electrolyte has been modelled either by using (i) analytical approach or (ii) numerical simulation, and both are discussed in this section.

2.1. Analytical approach

An early efforts of analytically modelling corrosion mechanisms by considering evaporating droplet electrolyte residing on a metal

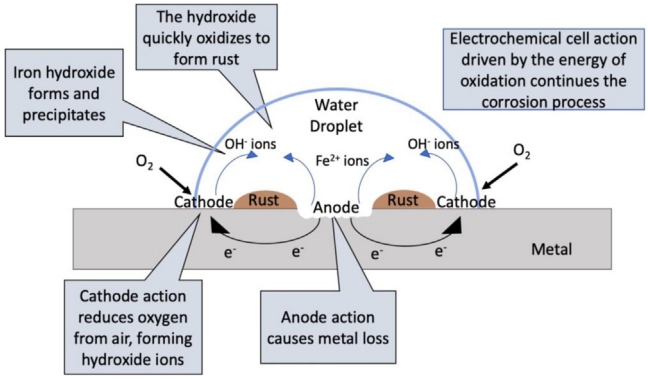

Fig. 2. Schematic of corrosion of metal (iron) under droplet electrolyte cross section.

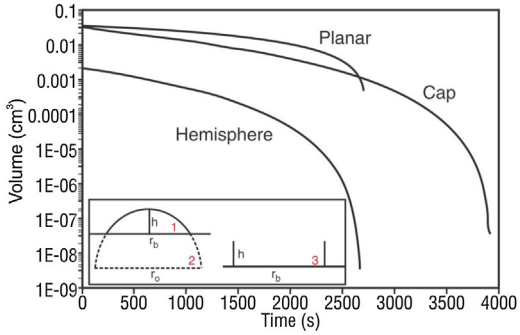

Fig. 3. Droplet volume as a function of evaporation time. Inset: Cross-section of 1. hemispherical, 2. flattened hemispheric cap and 3. planar cylindrical droplet geometries [17].

surface was done by Lyon et al. [17]. They developed a model of an evaporating droplet to simulate wetting and drying effects during atmospheric corrosion. The droplet size, anode-to-cathode resistance, oxygen reduction current and ohmic drop were calculated as a function of evaporation time. They considered three geometries as a representation of the droplet electrolyte; hemispherical, a flattened-hemispherical-cap and a planar (cylindrical) as shown in the inset of Fig. 3.

The influence of droplet evaporation on oxygen diffusion was described using Fick's laws. The electrolyte conductivity was modelled using Debye-Huckel-Onsager equation [75]. They assumed an arbitrary quantity of ionic species and fixed ratio of cathode to anode area (A_c/A_a). The results were computed for both evaporating and non-evaporating conditions. Fig. 3 shows the evolution in droplet volume as a function of evaporation time. During the evaporation of hemispherical and flattened-hemispherical-cap droplet, the anode-to-cathode resistance decreased as a function of evaporation time for both the hemispherical droplet due to increased conductivity of electrolyte as shown in Fig. 4(a). Although the oxygen reduction current density increased substantially during the evaporation, the total current decreased due to the reduced cathode area as shown in Fig. 4(c). In case of planar droplet geometry, the anode-to-cathode resistance was invariant with time as shown in Fig. 4(a) and the total oxygen reduction current increased as the cathode area did not change with evaporation time as shown in Fig. 4(c). Therefore, the anode-to-cathode resistance did not limit the corrosion rate in case of hemispherical droplet. However, for an electrolyte of uniform thickness (planar droplet geometry), the corrosion rate showed a tendency to become subjective to resistive control at a later stage of evaporation as shown in Fig. 4(b).

Whereas, for a non-evaporative condition in which the electrolyte concentration stayed constant, represents the situations where the condensed droplet is in equilibrium with the surrounding relative humidity and the surface is typically wet. The anode-to-cathode iR drop was invariant for the hemispheric droplet for a given concentration of electrolyte, irrespective of the droplet size as shown in Fig. 4(d). In case of uniform thickness electrolyte (planar droplet geometry), the iR drop rapidly increased with reduction in electrolyte thickness as shown in Fig. 4(d), which is same as in the case of evaporative condition but at a higher rate. Therefore, during non-evaporative conditions, the corrosion rate was under resistive control for both hemispherical and planar droplet geometries, but more predominant in case of uniform thickness electrolyte (planar droplet geometry). Although the effect of changing droplet geometry and increasing electrolyte concentration due to evaporation was studied in this work, it only gives the qualitative trends of anode-to-cathode resistance and total oxygen reduction current. Also, they consider the initial droplet radius to be 1 mm, which includes only a certain population of droplets as condensation is a multiscale phenomenon [55,61]. They also did not consider the influence of contact angle of the droplet which can have a significant influence on corrosion mechanism because the length of the diffusion path varies with geometrical changes [76].

Later, Jiang et al. [49] proposed an improved quantitative analytical steady-state model of corrosion under a hemispherical droplet by including the thickness of the static diffusion layer of oxygen in a droplet with a contact angle less than 90°. The model was based on their experimental findings to predict the effect of droplet distribution of equal size (termed as ïliquid dispersion¨) on the atmospheric corrosion rates. They divided the electrochemical reaction zone under the droplet electrolyte into bulk zone and a three-phase boundary (TPB) zone. They defined the three-phase boundary (TPB) zone for a droplet electrolyte as a two-dimensional liquid zone immediately inside the gas/liquid/solid phase boundary with the electrolyte thickness (δ) ranging from 0 to 100 μm as shown in Fig. 5(b). This is because the thickness of the static diffusion layer is generally agreed to be 100 μm [77].

Similarly, the bulk zone was defined as a two-dimensional liquid zone in which δ is greater than 100 μm. They established a relationship between the liquid dispersion and geometric properties of TPB zone as 'b' given by the Eq. (1). For the width of the TPB zone to be finite, the contact angle must be less than 90°. They conducted experiments on A3 steel and 304 stainless steel which were partially immersed in electrolyte to create a TPB zone for different TPB lengths as shown in Fig. 5(a). Experiments indicated that the effect of 'g' on the cathodic process only depended on the electrochemical process, independent of material properties. It was also found that the cathodic limiting current density nearly doubled with increasing 'g'.

$$b = \frac{S_{3B}}{S} = \frac{L \cdot 100\mu\text{m} \cdot \cot\theta}{S} = g \cdot 100\mu\text{m} \cdot \cot\theta \quad (1)$$

The model of Jiang et al. [49] established a relationship between the cathodic current density and the TPB length. The cathodic processes in both zones are under oxygen diffusion control at overpotentials which corresponds to the limiting diffusion current density plateau. Hence, a part of the total cathodic limiting current (i_d) flows through bulk and another component through TPB zones as described in Eq. (2).

$$i_d = i_{bulk} + i_{3B} \cdot b = nFD\left[\frac{C_{O_2,bulk}}{100\mu\text{m}} + \frac{C_{O_2,3B}}{\delta}\right] \cdot g \cdot 100\mu\text{m} \cdot \cot\theta \quad (2)$$

The calculated and experimental results of cathodic current densities at given polarization potential as a function of 'g' were compared as shown in Fig. 6 and are in good agreement. Therefore, Eq. (2) predicts that i_d linearly increases with increasing value of 'g'. It was also demonstrated that the increase in liquid dispersion on the surface leads to increase in total cathodic limiting current.

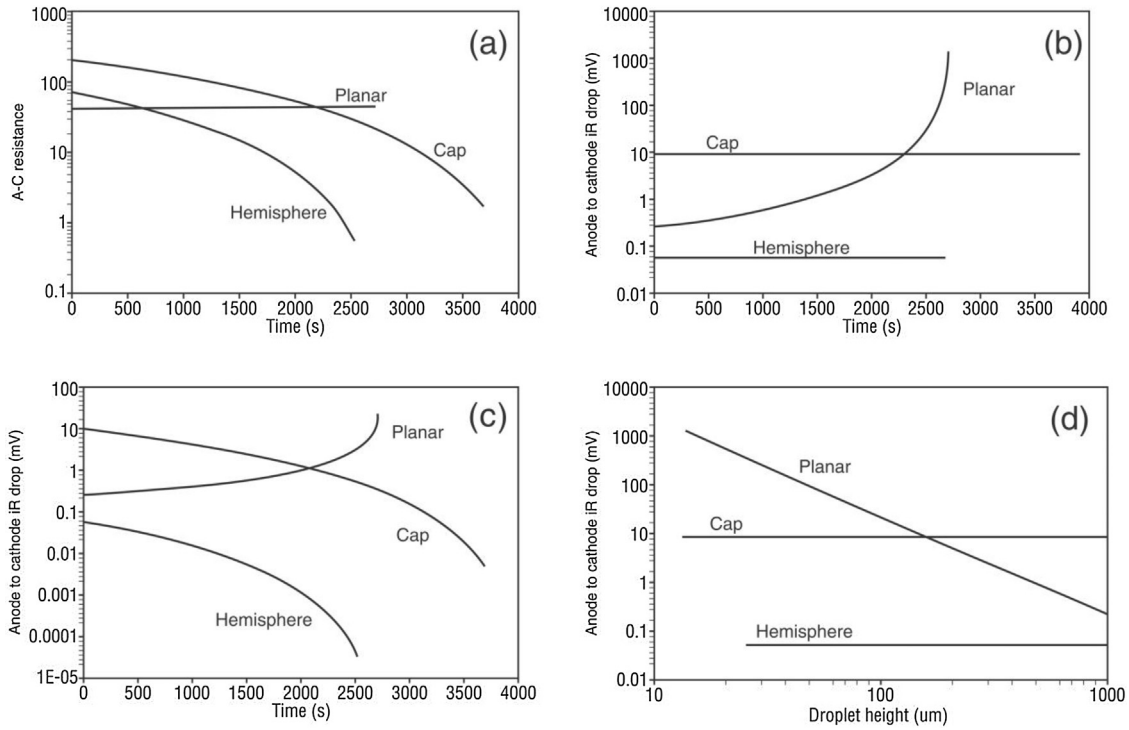

Fig. 4. (a) Anode-to-cathode resistance, (b) anode-to-cathode iR voltage drop and (c) total limiting oxygen reduction current as a function of evaporation time (increasing concentration of electrolyte), (d) anode-to-cathode iR voltage drop as a function of droplet height (assuming constant concentration) [17].

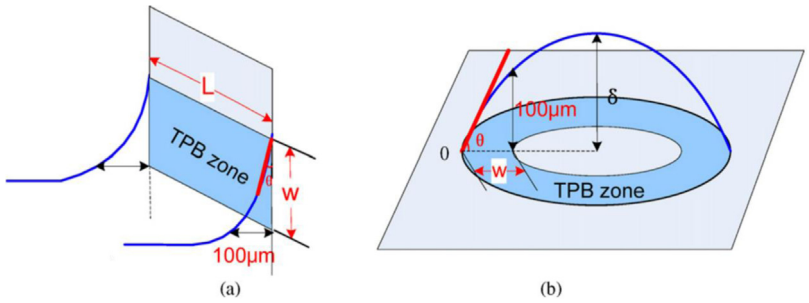

Fig. 5. The schematic diagram of the geometry of TPB zone. (a) A vertical electrode under partial immersion in electrolyte and (b) an electrolyte droplet attached on a planar electrode surface [49].

Table 1
Comparison of key differences between analytical modelling approaches of corrosion under droplet electrolyte.

No.	Approach	Key considerations	Key outcome	Shortcomings
1	Analytical by Lyon et al. [17]	(1) Evaporating droplet. (2) Wetting and drying effects. (3) Different droplet geometries. (4) Oxygen diffusion by Fick's law. (5) Electrolyte conductivity by Debey-Huckel-Onsager equation.	Evaporative condition: (1) For hemispherical droplet: anode-to-cathode resistance did not limit the corrosion rate. (2) For planar droplet: corrosion rate was subjective to resistive control. Non-evaporative condition: Corrosion rate was under resistive control for all geometries.	(1) Gives a qualitative trend but not quantitative understanding. (2) The initial droplet radius is always 1 mm. (3) Arbitrary quantity of ionic species. (4) Fixed ratio of cathode to anode area.
2	Analytical by Jiang et al. [49]	(1) Droplet divided into bulk and three phase boundary (TPB) zones. (2) Droplet contact angle (<90 deg.) (3) Droplet distribution (liquid dispersion). (4) Relationship between liquid dispersion and TPB length. (5) Relationship between cathodic current density and TPB length.	(1) The effect of TPB characteristic length ('g') on cathodic process was depended only on the electrochemical process, independent of material properties. (2) Calculated cathodic limiting current density linearly increases with increasing' g'. (3) Increase in liquid dispersion on the metal surface leads to increase in total cathodic limiting current.	(1) Limited to a contact angle between zero and ninety degrees. (2) Assumes equal drop-size distribution to account for liquid dispersion during atmospheric corrosion. (3) Static droplet.

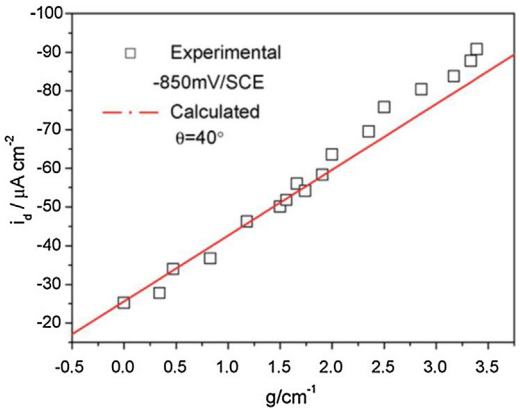

Fig. 6. Comparison between simulation result and experimental data simulation for the model validation [49].

Eq. (2) proposed by Jiang et al. [49] does well in estimating the cathodic limiting current density by considering the effect of the TPB zone and liquid dispersion which is importance in estimating the atmospheric corrosion rate. The model considers the droplet with a contact angle between zero and ninety degrees which was not taken into account by Lyon et al. [17]. In reality, the contact angle can be either less or more than ninety degrees depending on the surface physiochemical properties and contaminants present on the metallic surface [78]. The concept of dividing the TPB zones among equally sized droplets to account for liquid dispersion during atmospheric corrosion is an advantage of this model compared to the one by Lyon et al. [17]. But the model assumes equal drop-size distribution. In practice, the droplets of various sizes are distributed on the surface depending on the surface properties and environmental parameters like temperature and relative humidity [61,79]. Additionally, the distance and interactions between two adjacent droplets which can influence the drop-size distribution are not considered [80]. The model considers the static conditions and needs to include the description of how the droplet geometry, composition and contact angle evolve to be able to comprehensively estimate the atmospheric corrosion rates. Considering these approximations, the model describes the atmospheric corrosion process only partially. The summary of the discussed analytical models is described in Table 1.

2.2. Numerical simulations

A three-dimensional transient finite element model (FEM) describing the spatio-temporal variation of involved ionic species concentration within the electrolyte was developed by Venkatraman et al. [50,81]. The model considered corrosion of metal surfaces under a droplet, using a configuration similar to the case of the Evans drop experiment. They modelled corrosion under a droplet deposited on a bare metal surface in the absence of oxide or any other films. They simulated the early stage of corrosion before the formation of precipitates.

Although the model considered zinc in particular, it can be extended to simulate the corrosion process of different metals with corresponding input parameters and reactions. The flux of the involved species was given by the dilute solution theory [82] and the anodic/cathodic reactions were modelled using the Butler-Volmer relation [34]. The model assumed that no heterogeneous or homogeneous chemical reactions occur in the droplet. The concentration of the zinc ions was predicted to be high near the metal surface, with an accumulation towards the cathodic region. This is because of the fact that the model does not consider the scavenging mechanisms like precipitation of corrosion products. The simulation results showed how the current within the droplet enters from the anodic region and terminates in the cathodic region. However, the anode-cathode separation and its evolution with time were not described. Moreover, the model does not consider effect of natural convection within the droplet [83], which, depending on the size of the droplet, can have a significant influence on the movement of involved species within the droplet [84,85].

Later, more advanced but a two-dimensional transient finite element model including coupled, nonlinear, diffusion equations for ionic species, which included the contribution of migration, formation of primary precipitates, local electroneutrality and homogeneous reaction was developed by Chang et al. [86]. They modelled corrosion under a droplet placed on an iron surface. More importantly, the presence of anodic and cathodic regions was determined by the local potential distribution caused by the formation of differential aeration cells, and hence the location of anodic and cathodic regions was not assumed a priori but was a result of the numerical simulation. The active-passive transition for the anodic reaction was also not assumed a priori, but was instead obtained from coupling of the hypothesized surface and homogeneous reactions. Their model was subdivided into three parts: electrochemical reactions, convection equation and chemical reactions, and formation and influence of precipitates. The cathodic and anodic reactions were assumed to be reduction of oxygen and iron dissolution, respectively. The active-passive transition was assumed to be the consequence of the formation of corrosion products. Passivation was included in the kinetic current density 'i_k', Eq. (3), by allowing the fractional surface coverage of the corrosion products 'γ' to weight the contribution of passive active current densities. The concentration of dissolved oxygen was considered to be $C_{O2} = 0.284\ \text{mol m}^{-3}$ and five ionic species were assumed to be present in the solution: K^+, NO^{3-}, Fe^{2+}, H^+ and OH^-.

$$i_{k,Fe} = (1-\gamma)\cdot K_{0,Fe}\cdot \exp\left[\frac{2.303}{\beta_{Fe}}(\Phi_m - \Phi_0)\right] + \gamma \cdot i_{p,Fe} \quad (3)$$

Calculations were performed both at the corrosion potential (open-circuit) and at an applied potential using non-linear equations. Due to greater accessibility of oxygen, the cathodic area dominates at the periphery of the droplet and extends to the center similar to the results of Evan's drop experiments. Ferrous ions produced by the anodic reactions at the center react with the hydroxide ions from the cathodic reactions to form ferrous hydroxide. $Fe(OH)_2$ reacts with the excess OH^- to form $Fe(OH)_3$, which is an insoluble iron hydroxide complex that can dehydrate to form rust. Galvanic effects were seen to result from the formation of precipitates. A slightly alkaline region was seen at the periphery of the droplet due to the cathodic region and the center showed slightly acidic as a consequence of the formation of precipitates. The anodic region showed active-passive transition as a consequence of the formation of $Fe(OH)_3$ precipitates, but the cathodic reaction was still active. The shift of the passivated area can be seen in the changes of total current density shown in Fig. 7.

Similarly, the droplet corrosion simulation model containing dissolved CO_2 was also developed and found that the species $FeCO_3$ accumulated in the anodic reaction dominated area because the carbonate was the product of a homogeneous reaction [87]. Although the droplet corrosion model developed by Chang et al. [86] provides a framework to study the interactions among chemical and electrochemical reactions, deposition of corrosion products and transport, building an extension of the model to three-dimensions including the spacio-temporal variation of species can make it complete. In the atmospheric corrosion perceptive, the model could be extended to include the effect of the evolution of droplet size due to condensation and evaporation phenomena, the variation of contact angle with the wettability of the surface.

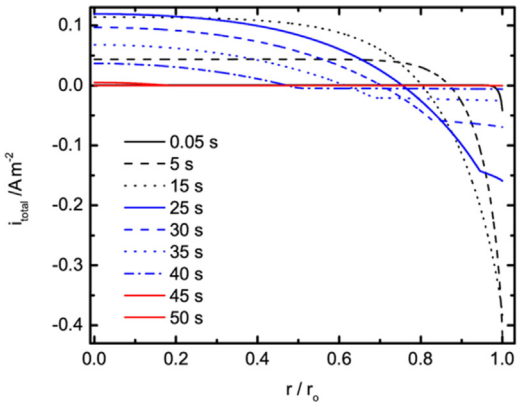

Fig. 7. Radial distribution of total density at the electrode surface with time as parameter [86,158].

The models [49,81,86,87] discussed so far focused on modelling the Evans drop experiment and have made a significant contribution towards understanding and mathematically simulating corrosion under droplet electrolytes. However, they only consider static conditions of the droplet electrolyte. It is important to account for the dynamic evolution of the droplet geometry because it was observed to have an influence on corrosion mechanisms [24,88].

Cole et al. [50] have focused on the development of a process-based model that defines the electrochemical and chemical processes that occur on a metal surface under a saline drop as a function of metal microstructure and oxide development [89]. It was found that the porous oxide layer in the zinc system promoted longer wetting times, facilitating oxygen reduction reaction [90,91]. These oxide layers are effectively grown in alkaline condition of bulk electrolyte, yet they are formed under droplet in neutral conditions [89,92,93]. This was expected to be due to the development of porous oxide that promotes sufficient alkalinity at the oxide-metal interface to promote the formation of a compact layer [89]. Therefore, two models named 'the droplet model' and 'the porous oxide model' were developed to account for the same processes. Additionally, the model developed by Venkatraman et al. [81] was extended to include variation of oxygen concentration as a function of droplet size. Fig. 8 shows the oxygen concentration in the droplet as a function of kR/D, where, 'k' is the cathodic reaction rate constant, 'R' is the radius of the droplet, and 'D' is the diffusion coefficient of dissolved oxygen. It was found that for a large drop, depletion of oxygen leads to preferential cathodic activity at the droplet edge. Whereas for a small drop, the oxygen concentration remains relatively uniform, and therefore cathodic activity is not controlled by the droplet geometry. Measurements by Cole et al. [92] on Zinc surface indicated that under a saline drop, a porous oxide thickness of around 1 μm was developed after 15–30 min. It was also found that the formation of a porous oxide dramatically influences the electrochemical activity on a metal surface as the oxide can, in some cases, support cathodic activity. The summary of the discussed numerical models is described in Table 2.

From the considered literature, it is clear that the geometry of the droplet electrolyte and its evolution play an important role and can lead to a variety of corrosion mechanisms [21,23–25,37,93]. Additionally, there are experimental results that report a deviation from the Evans drop behavior such as secondary spreading [10,23,25] and filiform corrosion [37], that has to be taken into consideration by the model in order to simulate atmospheric corrosion as it occurs. The holistic modelling approach for quantifying atmospheric corrosion rate to a reasonable accuracy needs to consider all possible physical, chemical and electrochemical mechanisms as a function of:

a) Dynamically varying droplet geometry [50].
b) Porous oxide layer and physio-chemical properties of the surface [90,91].
c) Active-passive transition due to formation corrosion products [86].
d) Environmental parameters [20] (such as humidity, temperature and presence of salts) on formation, distribution and evolution of droplet electrolyte [17,90,91,94].

Hence the subsequent sections are dedicated to an overview of modelling approaches to describe the formation and geometric evolution of droplet.

3. Modelling of formation and evolution of droplet

According to thermodynamics, the vapor to liquid phase transition occurs when the chemical potential of water vapor exceeds the chemical potential of liquid water. This condition occurs when the surface temperature is below dew point temperature or if the vapor pressure is increased above saturation pressure. The surface temperature of the metal exposed to the changing atmospheric conditions can drop below the dew point during the night and hence have droplet electrolyte adsorbed on the surface due to condensation.

The initial stage of condensation is a stochastic phenomenon at an atomistic scale which involves nucleation of water molecules on the surface to form clusters. These clusters diffuse along the surface and aggregate to form nuclei of water droplets that are distributed on the condensing surface. The nuclei are thermodynamically stable when the radius of the droplet reaches a certain critical value so that the formation work of the condensate on the surface is positive and hence the Gibbs free energy is negative [55,95]. These thermodynamically stable nuclei are pinned on the surface and initially grow in size by direct condensation of water molecules from air onto the droplet nucleus and by aggregation of smaller clusters that are less stable. During the vapor to liquid phase transition, the diffusion of new vapor molecules onto the adsorbed droplet nucleus is influenced by its curvature [96]. The curvature of the droplet is determined by the contact angle which is a function of surface free energy [55]. As the droplets grow in size, they come in contact with adjacent droplets and merge to form a bigger droplet. The merging frequency is propositional to the density of droplet distribution on the surface and temperature difference between the environment and the surface (termed as degree of subcooling). The merging of adjacent droplets is due to the inter-molecular force of attraction and is known as coalescence. In case of a flat surface, the growth of droplets with time leads to a transition of dropwise to filmwise condensation at total surface coverage, which is proportional to degree of subcooling [18]. The condensation of atmospheric moisture constitutes of nano, micro, meso and macroscopic processes which have been modelled in a multiscale approach [61].

3.1. Nucleation and growth of droplet electrolyte

Depending on the approach used in the simulation of initial stage of condensation, models can be categorized into two groups, namely, atomistic and continuum models. The atomistic modelling is a discrete approach which considers all kinds of nucleation. Whereas, the continuum modelling approach considers instantaneous nucleation of droplets based on deterministic description.

3.1.1. Atomistic approach

In case of atomistic modelling approach, it considers adsorption of every single or a set of molecules on the condensing surface known as monomers. The adsorbed monomers undergo a

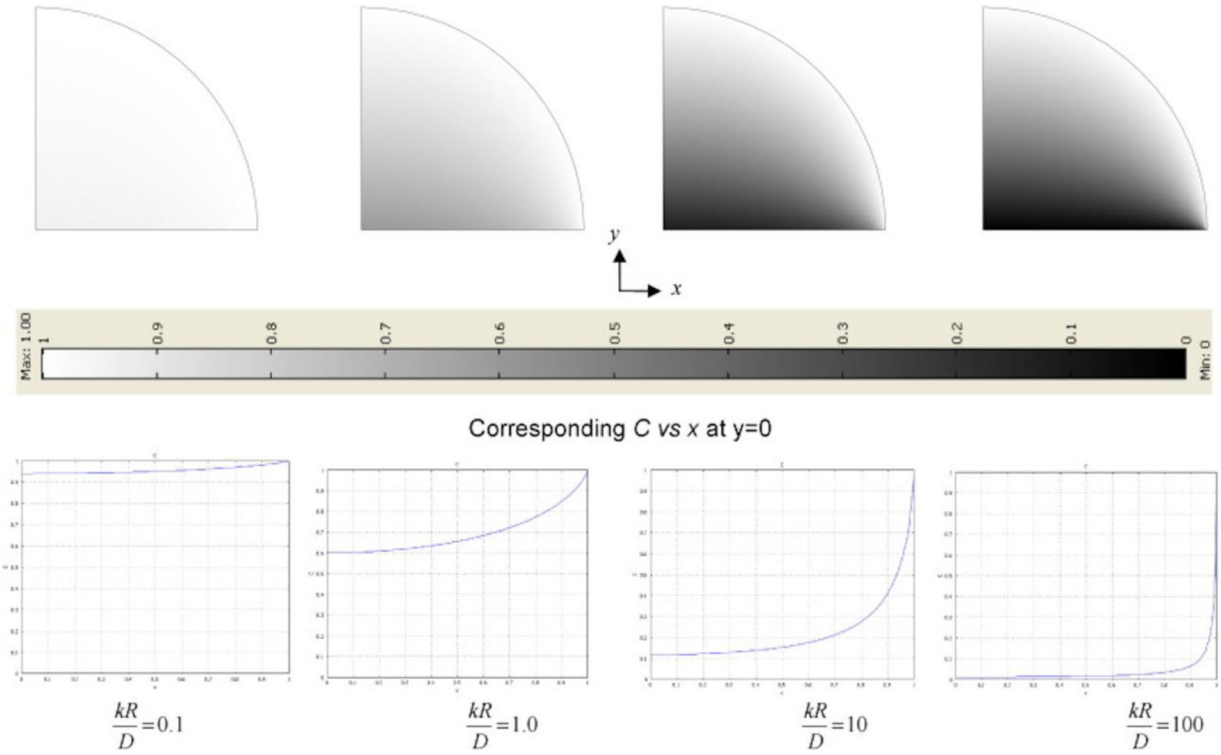

Fig. 8. Oxygen concentration in the droplet as a function of kR/D, where 'k' is the cathodic reaction rate constant, 'R' is the radius of the droplet, and 'D' is the diffusion coefficient of dissolved oxygen [50].

Table 2
Comparison of key differences between numerical modelling approaches of corrosion under droplet electrolyte.

No.	Approach	Key considerations	Key outcome	Shortcomings
1	Numerical simulation by Venkatraman et al. [50,81]	(1) Three-dimensional transient finite element model. (2) Droplet on bare zinc surface in the absence of oxide layer. (3) Spatio-temporal variation of ionic species concentration. (4) Early stage of corrosion: no formation of precipitates.	(1) Concentration profile of zinc ions and plot of current density vectors. (2) Concentration of the zinc ions was high near the metal surface, with an accumulation towards the cathodic region.	(1) Does not consider heterogeneous or homogeneous chemical reactions in the droplet. (2) Static droplet. (3) Anode-cathode separation was not described.
2	Numerical simulation by Chang et al. [86]	(1) Two-dimensional transient finite element model of droplet on iron. (2) Contribution of migration; primary precipitates; local electroneutrality and homogeneous reaction. (3) Anodic and cathodic regions were not assumed prior. (4) Active-passive transition due to corrosion precipitates. (5) Simulated both at corrosion and at an applied potential. (6) Extended to simulate corrosion in the presence of CO_2 instead of O_2.	(1) Galvanic effects due to precipitates. (2) Alkaline cathodic region at the periphery and slightly acidic at the center. (3) Active-passive transition of anode due to of $Fe(OH)_3$ precipitates, with active cathodic region. (4) With dissolved CO_2 found that the species $FeCO_3$ accumulated in the anodic reaction	(1) Static droplet. (2) Needs extension to include parameters like surface wettability and spatio-temporal variation of involved ionic species with 3D model.
3	Combination of empirical and numerical simulation by Cole et al. [50]	(1) Multiscale model w.r.t. production, transport, and deposition of aerosols. (2) Dynamic droplet. (3) Spatio-temporal variations of involved ionic species. (4) Porous oxide layer.	(1) Oxygen concentration in the droplet as a function of droplet radius, cathodic reaction rate constant, diffusion of O2. (2) Porous oxide promotes sufficient alkalinity at the oxide–metal interface, promoting the formation of a compact oxide layer.	(1) Empirical models describing transport of aerosols doesn't give a general understanding. (2) Droplet model needs extension to include surface energy and evolution of anode-cathode separation. (3) The porous oxide model needs extension to account for oxide layer evolution due to corrosion precipitates and pH variations within the droplet.

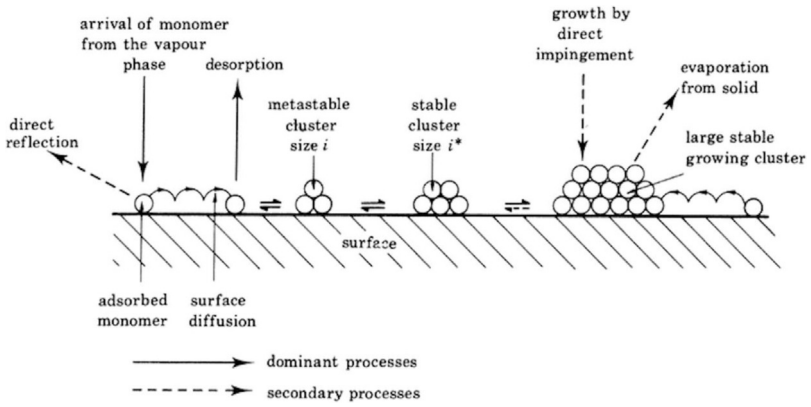

Fig. 9. Schematic of distribution of cluster on substrate [98].

sequence of processes such as adsorption, surface diffusion, desorption, agglomeration, transfer of energy, and formation of clusters, all occurring in parallel at different scales [97,98] as shown in Fig. 9. Clusters that reach a certain critical size will form a stable nucleus of water which is in thermodynamic equilibrium with the surface and the surroundings, eventually manifesting as a distribution of droplets on the condensing surface. Initially, the droplet grows in size due to direct condensation viz., attachment of water molecules from vapor onto the droplet surface. As the droplets grow from nano and microscale to macroscopic scale, the droplets grow mainly due to coalescence.

During the earlier efforts of simulating condensation phenomenon, the understanding of nucleation of liquids from the vapor phase was dominated by classical nucleation theory (CNT) [98–101]. The CNT uses the capillary approximation where the free energy of the stable nucleus is determined by considering it as a macroscopic droplet and free energies of the surface relative to the background vapor [102]. The surface free energy is estimated from the surface tension of an equilibrium liquid-vapor interface. The effect of the solid surface on the nucleation process was evaluated by considering the solid-liquid interfacial energy into the calculation of nucleation free energy. By doing so, the heterogeneous nucleation rates were obtained from CNT model [103,104]. However, it was found that CNT fails to describe the nucleation of clusters smaller than eight water molecules [105]. To overcome these limitations of CNT, in recent years, Monte Carlo (MC) and Molecular Dynamics (MD) methods have been developed to simulate the nucleation process considering direct molecule interactions [106–108]. According to MC simulation, the CNT overestimates the formation free energy of the critical cluster and underestimates the droplet size at temperatures near the triple point [109]. But in case of MD simulation, the predicted critical size of the droplet nuclei matched the values from the CNT at low temperatures.

During the vapor-liquid phase transition, the saturated molecules in contact with surface cooled below the dew point are adsorbed on the surface by losing their latent heat and diffuse along the surface. Some of these active molecules go back to vapor phase because of the desorption due to the combined effect of temperature, vapor pressure, surface wettability and roughness. During this initial stage, the attachment of water molecules to the clusters adsorbed on the surface has to dominate the desorption process to have a net nucleation of the molecules. The energy barrier for nucleation depends on the surface wettability, surface tension and binding energy, which are characterized by the droplet contact angle on the surface. Higher contact angle results in higher adsorption energy barrier, which means that the surface requires higher degree of cooling to have an adsorption of water molecules [55]. The surface tension at the liquid-solid interface and inter-molecular interaction between two adsorbed water molecules drive the formation of aggregates and eventually a stable nucleus [97]. Wang et al. [110] described the aggregation process on the basis of mean chemical potential of the active molecules and fundamental equation of self-aggregation thermodynamics in 1D, 2D and 3D. It was found that there exists a critical aggregation concentration (CAC) of active molecules below which all the active molecules exist as monomer. When the monomer concentration equals CAC, aggregation of active molecules is initiated, and the concentration of aggregates increases rapidly with the increase in total concentration. The aggregation of active molecules will lead to formation of cluster. The cluster can either grow further by addition of more active molecules or decay, depending on the thermodynamic stability of the cluster. From the transient nucleation size distribution model, Xu et al. [111] found that the cluster growth/decay was significantly affected by the surface free energy of condensing surface. As the stable nuclei of droplets grow in size, the dimensions of consideration shift from nanoscale to micro, meso and macroscales.

To simulate the condensation phenomena that occur at different scales, Sikarwar et al. [61] developed a multiscale modelling of condensation where the critical radius of the droplet during condensation of saturated vapor on a sub-cooled substrate was estimated using the population balance model. The model predicted the distribution of stable cluster sizes under steady-state conditions. However, the nucleation regime was modelled by neglecting the effect of evaporation of molecules back to the vapor state. Equations that depict the time rate of variation of number density of monomers, cluster density with atoms and of saturation island density were used for numerical simulation of nucleation regime [112–114]. The largest stable cluster size in the number density distribution was taken to be representative of the minimum drop radius (stable nuclei) formed in a dropwise condensation process. Results show that the number density distribution was sensitive to the surface diffusion coefficient of the clusters and the rate of vapor flux impinging on the substrate [61]. The minimum drop radius increased with the diffusion coefficient and vapor flux but with rather weak dependency [61].

Later, Xu et al. [111] developed a transient nucleation model to describe the nucleation process based on first principles. The evolution of cluster/droplet size distribution based on molecular kinetic theory was modelled and the influence of the contact angle on the condensation phenomena based on classical capillarity approximation was taken into account. In this model, the attachment and detachment frequencies of molecules to/from the cluster surface were used to describe the growth/decay of the cluster size and subsequently the evolution of cluster size distribution was obtained. The main assumptions in this model were that the nucle-

ation occurs only at the nucleation site and physical properties of the cluster were described by classic capillarity approximation. The growth of the cluster was considered as a binary reaction between n-sized cluster and monomer as shown in Eq. (4). Where, k_n^+ and k_n^- are the attachment and detachment frequencies of monomer respectively to/from the n-sized cluster surface.

$$n \text{ cluster} + \text{monomer} \underset{k_{n+1}^+}{\overset{k_n^+}{\rightleftharpoons}} n+1 \text{ cluster} \tag{4}$$

From the considered literature, it is clear that the formation and growth of droplet nuclei at an atomistic scale are mainly a function of concentration of adsorbed monomers, surface free energies and surface diffusion coefficient of the clusters. Moreover, the MC and MD simulation results were highly dependent of the choice of molecular interaction potential model [115]. The implementation of atomistic scale models to simulate the condensation process on large surfaces can be both challenging and computationally expensive. Therefore, to be able to efficiently simulate the corrosion process under droplet electrolyte by considering the process of formation and evolution of the droplet, it is important to know the minimum droplet size above which corrosion is significant. More investigations are required to be done to estimate the corrosion rate at different droplet sizes for a given metal, pH and salinity of the droplet. Based on the relevant droplet size, appropriate condensation modelling approaches have to be carefully chosen. The computational cost is also of prime importance because, in practice, the holistic corrosion model should be able to estimate the corrosion rate of an essentially varied and larger surface area. Cole et al. [93] studied corrosion of zinc surfaces caused by fine size acidified droplets of diameter ranging from ~0.1–5 μm. The corrosion was found to be a function of surface area to volume ratio, oxygen diffusion and microstructural features of the metal. Whereas, according to the experimental investigation of corrosion due to NaCl droplets on carbon steel done by Li and Hihara [24], the corrosion was significantly reduced for droplet diameter less than 45 μm which is quite a big dimension at atomistic scale. Hence, it is worth considering computationally inexpensive, yet well descriptive continuum approaches in relative to atomistic approaches.

3.1.2. Continuum approach

The continuum approach is based on the assumption of instantaneous nucleation and focuses on describing the growth of the droplets with thermodynamic equations of heat and mass transfer [116–118]. Definite number of randomly distributed nucleation site density is considered based on experimental findings [79,80]. The evolution of the droplets' distribution on the surface is described by various random distribution functions and algorithms [57,79,80,118]. The droplets initially grow by direct condensation of water molecules from the vapor until they reach the critical coalescence radius and then grow mainly by coalescence effect [61]. This is because smaller droplets offer less thermal resistance and thus promote rapid condensation. On the other hand, the larger droplet has higher thermal resistance and hence grows mainly due to coalescence [65]. Coalescence plays a major role in determining the drop size distribution during condensation. It was demonstrated that coalescence is also affected by contact angle, especially for two droplets with significantly different sizes [65].

Early simulation of dropwise condensation to estimate the heat transfer coefficient was done by considering active nucleation site density between 10^5-10^9 sites/cm^2 [119–121]. The models considered the condensation as a steady process and omitted the influence from contact angle variations at macroscopic level. They assumed the drop to be always hemispherical in shape. However, dropwise condensation is inherently a transient phenomenon involving the evolution of the size and distribution of the droplets. To account for the inherently transient nature of dropwise condensation, Tanaka [122] developed a transient numerical model to simulate the drop size distribution and the growth rate of droplets by taking the statistical and geometrical conditions into account. It was seen that the drop-size distribution curve had a characteristic profile in the range of comparatively large drops after a certain time, which was referred to as a 'universal distribution of large drop range'. The growth rate of individual droplets was modelled using the heat flux through a single droplet including contact angle [61,123]. Spatial droplet distribution and surface coverage at different angles of substrate inclination was estimated by the simulation [61]. The drop size distribution was seen to follow the power law.

Later, Qi et al. [124] proposed random fractal models to describe the drop-size distribution of direct condensation drops and coalescence drops on a condensing surface. The effect of the contact angle and its hysteresis, the nucleation site density, the fractal dimension for drop sizes and, maximum and minimum drop radii were considered. The simulation results also indicated that the fractal dimension for drop size distribution decreases with increasing contact angle.

Recently, Barati et al. [79] developed a model to simulate the spatial distribution of droplets during dropwise condensation. The effect of surface temperature (T_s) and initial nucleation site density (N_D) on the area occupied by the droplets was studied. The simulation algorithm was initiated with distribution of droplets based on ṗoisson point processänd investigated the spatial coverage of droplets using Ripley's function method with experimental comparison. The minimum radius [125] (critical radius) of the droplet that is able to grow is given by Eq. (5). The evolution of average radius and density of droplets simulated by the model was a function of initial nucleation density assumed and was in good agreement with the experiments. It was noted that the surface coverage of the droplets was a strong function of initial nucleation density considered in the model and less dependent on surface temperature. However, the model assumes homogeneous distribution of droplet which may not be the case in reality because the surface defects on the surface act as a preferential nucleation site.

$$r_{\min} = \frac{2\sigma_{lv} T_s}{H_{lv} \cdot \rho \cdot \Delta T} \tag{5}$$

Xu et al. [80] developed a simulation model which considered the 3D profile of the droplet. They initialized the simulation with fixed nucleation sites that were randomly distributed on a condensing surface and nucleation sites are occupied by initial droplets. The initial number of nucleation sites per unit area was considered to be 10^9-10^{13} sites/m^2. From both simulation and experiment, it was seen that 3D profile of the droplet can change the spatial distribution of the droplets. The smaller droplets were found beneath larger ones and these smaller droplets were also able to realize multiple coalescence and re-nucleation due to the significantly different sizes.

The continuum modelling approach for simulating the dropwise condensation is been continuously evolving for higher accuracy and efficiency of the algorithms for predicting the heat exchange coefficient, evolution of droplet size and its distribution on the surface, which are critical for heat exchanger design [79,111,122,124]. The physiochemical properties of the surface influence the liquid-solid interaction and hence the contact angle of the droplet. Additionally, contact angle influences the growth rate of the droplet and hence the heat flux. The random initial nucleation site assumed in the model influences the drop-size distribution and the surface coverage. The continuum condensation model does sufficiently well in describing the formation and growth of the droplet of dimensions for which the corrosion was significant [24]. The advantage of continuum modelling approach is the lower computational cost compared to the atomistic modelling approaches. Therefore, in

Table 3
Comparison of key differences between modelling approaches of formation and evolution of droplet.

No.	Approach	Features
1	Atomistic approach	Accounts for: Adsorption of monomers. Surface diffusion of monomers. Agglomeration Cluster formation Droplet nucleation. Mostly uses: Random distribution functions to describe the nucleation sites. Monte-Carlo or molecular dynamics simulations.
2	Continuum approach	Accounts for: Instantaneous nucleation of droplets. Growth of droplets further in macroscopic scale. Mostly uses: Randomly distributed nucleation sites.
3	Coupled approach	Heat and mass transfer formulations. Combination of atomistic and continuum approaches.

order to model atmospheric corrosion as a function of evolving droplet geometry, the continuum approach of describing the formation and growth of the droplet is computationally more relevant than the atomistic modelling approaches.

3.1.3. Coupled approach

To take advantage of both atomistic and continuum approaches, a coupled modelling approach was developed by Sikarwar et al. [61] to account for nano, micro and macroscopic scales of the condensation process. The size of the critical cluster estimated by the population balance model at atomistic scale was considered as the minimum droplet size in the continuum approach. Mamme et al. [126] developed a coupled model of finite element modelling (FEM) with random walk algorithm to describe the nucleation and growth process during electrodeposition. The model implicitly considers surface free energy factor and inter-facial binding through a so-called parameter mobility factor. Using similar approach, the model can essentially simulate the nucleation and growth of water molecules during condensation. Table 3 summarizes the main features of the discussed condensation modelling approaches.

3.2. Drying of droplet

Evaporation of droplet electrolyte increases the concentration of dissolved salts in the electrolyte, which decreases the anode to cathode resistance, total cathodic current and resistive losses [17,40,127,128]. To consider the corrosion due to atmospheric exposure, the concept of time of wetness (TOW) is often used. TOW is referred to as the period in which the metal surface stays sufficiently wet for corrosion to occur [31]. The drying rate of the metal surface determines the TOW and hence the possible duration of corrosion process. Therefore, it is important to model the evaporation of the droplet electrolyte and understand its implications on atmospheric corrosion mechanisms. Drying of droplet electrolyte is caused by the evaporation of condensed water molecules from the surface to vapor form. The electrolyte evaporates from the surface when the temperature of the surface rises above the dew point temperature, which is likely to occurs during the daytime, when the heat from the sun/surrounding heats up the metal surface. An early effort to model the evaporation of moisture from the metal surface using classical mass transfer theory was done by Cole et al. [94]. Time taken for drying of metal surface was found to be dependent on the airflow over the wet surface. For a lower airflow speed, the drying time was significant (6–12 h) and was influenced by the humidity. Whereas, a higher airflow speed led to faster drying (less than 1 h). The difference between surface temperature and ambient temperature also has a significant influence of drying time and is strongly influenced by presence of moisture on the surface, wind speed and cloud cover [129]. Mathematical models describing the variation of surface temperature of a metal due to different thermal processes such as conduction, convection and radiation, and their dependence on climatic parameters were developed by Cole and Paterson [35]. The heating of metal surface during the daytime depended on whether the sky is cloudy or not, evaporation rate, ambient relative humidity and temperature. When the sky is clear, the solar heating of a metal was initially observed to be suppressed by the cooling effects of evaporation which lead to a slower drying and contracting of droplets and films, while corrosion occurs [35,129].

Generally, there are two modes of droplet evaporation [130–132] (i) constant contact radius (CCR) mode, characterized by reducing of contact angle and pinning of contact line [133]. (ii) constant contact angle (CCA) mode, characterized by shrinking of contact line and extremely small variation contact angle [134]. The modes of evaporation are mainly determined by the surface roughness and contact angle of the droplet [135]. The CCR and CCA mode are generally observed when the droplet contact angle $\theta < 90^\circ$ and $\theta > 90^\circ$ respectively [136].

Numerical simulation of droplet lifetime (evaporation) is an ongoing research due to its variety of applications such as thin film coating, ink-jet printing and spray coating [137–141]. Most recent articles [142–144] discussed various approaches for theoretical estimation of evaporation rate considering evaporative cooling, marangoni flow [145] and contact line dynamics (stick-slip behavior) which has large influence on droplet evaporation. Marangoni flow is a thermocapillary-driven convection of water molecules within the droplet from a region of lower to higher surface tension [83,146,147]. The localized surface tension gradients within the droplet are a result of evaporative cooling of free surface. The continuous evolution of the free surface (the liquid-air interface) makes the droplet evaporation a transient phenomenon which is difficult to model as it involves complex moving boundary problem. Due to this complexity, a simplified steady-state evaporation model has been developed by considering the effect of latent heat of vaporization, thermal marangoni convection, and Stefan flow in the surrounding gas [148]. Results of modeling allow the characteristic droplet sizes to be estimated when each of the above-mentioned phenomena becomes important.

The transient nature of the droplet evaporation process was approximated by decoupling the free surface evolution from heat, momentum and mass transfer equations. This way, the moving boundary problems are converted to time series of fixed boundary problems [149,150]. Later, a transient and coupled numerical model considering transport process in solid, liquid and gas phases along with evolution of free surface was developed based on arbitrary Lagrangian-Eulerian (ALE) formulation [145]. It was noted that the evaporation flux was found to be inversely proportional to the droplet's contact angle [151]. Further improvement to the ALE based numerical model to include natural conversation for both heat and mass transfer was done [152] and found that the contribution of natural convection is significantly high of total contribution of convective mass transport in droplet evaporation.

The evaporation process is influenced by number of parameters such as contact angle, natural convection, marangoni flow, topography and thermal conductivity of the surface [145,151,152]. Significant efforts have been done to model and accurately predict the evaporation rate of a droplet [153–155]. Linking the corrosion mechanisms under droplet electrolyte with the models that describe evaporation and condensation of the droplet will possi-

bly give a complete understanding needed to better predict the atmospheric corrosion rates.

4. Discussion

The current state-of-the-art of mechanistic modelling of corrosion under droplet electrolyte has been presented in this review and is summarized in Tables 1–3. The review highlights all the aspects required for comprehensive modelling of corrosion process under droplets, to predict the corrosion rates due to long-term atmospheric exposure. As noted in the review, modelling of corrosion under droplet electrolyte is in an infancy stage and requires extensive work to be done. For a given metal, corrosion activity is a function of droplet dimension. There exists a certain dimension (radius/height) of the droplet electrolyte below which the corrosion is significantly reduced but does not stop [24,88]. Similarly, there also exists a maximum dimension (radius/height) of droplet electrolyte above which the corrosion is similar to bulk electrolyte corrosion. The range of minimum and maximum droplet diameter in which significant corrosion was observed [24] is between 103−426 μm, where the cathodic diffusion-limited oxygen reduction current density was found to be inversely proportional to the droplet size. A random distribution of anodic and cathodic sites was reported in the droplet on steel alloys [22] and more serious localized corrosion was observed when droplet size was increased. However, relatively reduced corrosion activity was observed in fine size acidified droplets with diameter ranging from ~0.1–5 μm [93]. Along with existing work [22,24,88,93], precise mapping of corrosion rate at different droplet sizes and salinity for different metals must still be done to draw a sound understand of the cathode/anode distribution and their evolution with time. The currently available droplet corrosion models do not include the combined effect of time on the geometry of the unstable droplets and corrosion, which is definitely a critical gap to be filled in order to proceed towards more complete atmospheric corrosion model.

The hygroscopic properties of the surface contaminants and their influence on the wetting/drying of metal surface are quite complex and are still to be considered in detail by the droplet corrosion models [17,49,50,81,87]. Therefore, the future work in modelling droplet corrosion also needs to consider both individual and consolidated effect of fundamental influencing parameters on corrosion mechanisms such as,

(1) Wetting of metal surface by aqueous droplets/films due to condensation and chemical adsorption of moisture due to hygroscopic properties of surface contaminant and salts.
(2) Influence of droplet size, their distribution and surface coverage on the corrosion activity.
(3) Formation of corrosion products and their influence on passivation and wetting/drying of the surface are yet to be clearly obtained.
(4) Influence of pH and porous/non-porous oxide layers on corrosion rate.

Additionally, as pointed out in the review, the corrosion rate increases as the droplet evaporates due to increase in concentration of the dissolved salts and reduced diffusion path of ambient oxygen to reach the corroding surface. Hence it is necessary to couple the condensation and evaporation process of the droplet electrolyte with corrosion mechanisms to have a multiscale holistic atmospheric corrosion model.

The existing droplet corrosion models [17,49,50,81,87] don not consider the surface energy factor and its influence on wettability of the surface. Therefore, future models must also consider the surface energy factor that dictates the wettability and contact angle of the residing droplet and hence the uniformity of diffusion of ambient oxygen in the droplet which influences the corrosion rates. Additionally, electrochemical active-passive transition due to the precipitation of corrosion products and oxide layers must also be taken into account as it can influence the prediction ability of the model. The precipitation can also alter the physicochemical properties of the surface, which possibly can change the contact angle of the droplet electrolyte and influence the condensation/evaporation rates. As seen from the overview of different modelling approaches to describe the droplet condensation and evaporation process presented in this review, the rate at which the geometry of the droplet is changed depends on multiple environmental factors such as temperature, humidity and surface energy. The variation of surface temperature and its mutual dependence on condensation and evaporation of surface droplets/film should also be investigated and modelled further at all possible atmospheric scenarios such as day/night, cloudy/clear sky and varying wind speeds. Findings from the condensation and evaporation models in the field of thermal energy applications along with pollutants and marine aerosol transport and deposit [156,157] can be brought together with droplet corrosion models to have a realistic description of the atmospheric corrosion mechanisms. Since the ultimate goal is to extrapolate the model to predict the lifecycle of a real structure exposed to atmospheric corrosion damage, it becomes critical to account for all the parameters influencing droplet corrosion mechanisms. Therefore, in our opinion, to ensure correct estimation of atmospheric corrosion rates, the influence of formation and geometric evolution of the droplet electrolyte, material microstructural and surface energy factors on the corrosion mechanisms needs to be considered in detail with a multiscale modelling approach and integrating the existing models together. Thus, predicting the component life to ensure materials are designed against relevant corrosive environments.

Acknowledgements

This work was financially supported by the European Union's Horizon 2020 Research and Innovation Programme under the Marie Sklodowska-Curie grant agreement (No. 764977).

References

[1] C. Leygraf, I.O. Wallinder, J. Tidblad, T. Graedel, Atmospheric Corrosion, John Wiley & Sons, 2016.
[2] C. Hansson, Metall. Mater. Trans. A 42 (2011) 2952–2962.
[3] G. Koch, Trends Oil Gas Corros. Res. Technol. (2017) 3–30.
[4] B. Hou, X. Li, X. Ma, C. Du, D. Zhang, M. Zheng, W. Xu, D. Lu, F. Ma, npj Mater. Degrad. 1 (2017) 4.
[5] G. Koch, J. Varney, N. Thompson, O. Moghissi, M. Gould, J. Payer, International Measures of Prevention, Application, and Economics of Corrosion Technologies Study, NACE International, 2016.
[6] J. Dong, E. Han, W. Ke, Sci. Technol. Adv. Mater. 8 (2007) 559–565.
[7] I.S. Cole, W. Ganther, J. Sinclair, D. Lau, D.A. Paterson, J. Electrochem. Soc. 151 (2004) B627–B635.
[8] I. Cole, N. Azmat, A. Kanta, M. Venkatraman, Int. Mater. Rev. 54 (2009) 117–133.
[9] J. Alcántara, D. de la Fuente, B. Chico, J. Simancas, I. Díaz, M. Morcillo, Materials 10 (2017) 406.
[10] Z.Y. Chen, The Role of Particles on Initial Atmospheric Corrosion of Copper and Zinc: Lateral Distribution, Secondary Spreading and CO2-/SO2-Influence, Ph.D. Thesis, KTH Royal Institute of Technology, 2005.
[11] I.S. Cole, W. Ganther, Corros. Eng., Sci. Technol. 43 (2008) 156–162.
[12] G. Tammann, W. Boehme, Ann. Phys. 414 (1935) 77–80.
[13] J.L. McCormick, J.W. Westwater, Chem. Eng. Sci. 20 (1965) 1021–1036.
[14] A. Umur, P. Griffith, J. Heat Transfer 87 (1965) 275–282.
[15] I. Cole, D. Paterson, Corros. Eng., Sci. Technol. 44 (2009) 332–339.
[16] E. Schindelholz, B. Risteen, R. Kelly, J. Electrochem. Soc. 161 (2014) C450–C459.
[17] S.B. Lyon, C.W. Wong, P. Ajiboye, An Approach to the modelling of atmospheric corrosion, in: Atmospheric Corrosion, ASTM International, 1995.
[18] J. Rose, Proc. Inst. Mech. Eng., Part A 216 (2002) 115–128.
[19] I.S. Cole, D. Lau, D.A. Paterson, Corros. Eng., Sci. Technol. 39 (2004) 209–218.

[20] N. Van den Steen, H. Simillion, O. Dolgikh, H. Terryn, J. Deconinck, Electrochim. Acta 187 (2016) 714–723.
[21] X. Tang, C. Ma, X. Zhou, X. Lyu, Q. Li, Y. Li, Electrochem. Commun. 101 (2019) 28–34.
[22] Y. Wang, W. Wang, Y. Liu, L. Zhong, J. Wang, Corros. Sci. 53 (9) (2011) 2963–2968.
[23] T. Tsuru, K.I. Tamiya, A. Nishikata, Electrochim. Acta 49 (2004) 2709–2715.
[24] S. Li, L. Hihara, J. Electrochem. Soc. 159 (2012) C461–C468.
[25] B. Risteen, E. Schindelholz, R. Kelly, J. Electrochem. Soc. 161 (2014) C580–C586.
[26] V. Kucera, E. Mattsson, Corros. Mech. 28 (1987) 211–284.
[27] J. Wisniewski, Water Air Soil Pollut. 17 (1982) 361–377.
[28] P.A. Schweitzer, Fundamentals of Metallic Corrosion: Atmospheric and Media Corrosion of Metals, CRC Press, 2006.
[29] P.A. Schweitzer, Atmospheric Degradation and Corrosion Control, CRC Press, 1999.
[30] R. Baboian, Synergistic effects of acid deposition and road salts on corrosion, in: Corrosion Forms and Control for Infrastructure, ASTM International, 1992.
[31] F. Corvo, T. Pérez, Y. Martin, J. Reyes, L. Dzib, J. González-Sánchez, A. Castañeda, Corros. Sci. 50 (2008) 206–219.
[32] E. Schindelholz, R.G. Kelly, Corros. Rev. 30 (2012) 135–170.
[33] C.M. Hangarter, S.A. Policastro, Corrosion 73 (2016) 268–280.
[34] C. Brett, A.M.O. Brett, Electrochemistry: Principles, Methods, and Applications, Oxford University Press, Oxford, 1993.
[35] I. Cole, D.A. Paterson, Corros. Eng., Sci. Technol. 41 (2006) 67–76.
[36] U.R. Evans, Ind. Eng. Chem. 17 (1925) 363–372.
[37] J. Weissenrieder, C. Leygraf, J. Electrochem. Soc. 151 (2004) B165–B171.
[38] Y. Wang, W. Wang, Y. Liu, L. Zhong, J. Wang, Corros. Sci. 53 (2011) 2963–2968.
[39] Z. Liu, W. Wang, J. Wang, X. Peng, Y. Wang, P. Zhang, H. Wang, C. Gao, Corros. Sci. 80 (2014) 523–527.
[40] T. Muster, A. Bradbury, A. Trinchi, I. Cole, T. Markley, D. Lau, S. Dligatch, A. Bendavid, P. Martin, Electrochim. Acta 56 (2011) 1866–1873.
[41] N. LeBozec, D. Thierry, A. Peltola, L. Luxem, G. Luckeneder, G. Marchiaro, M. Rohwerder, Mater. Corros. 64 (2013) 969–978.
[42] N. LeBozec, N. Blandin, D. Thierry, Mater. Corros. 59 (2008) 889–894.
[43] J.H. Ahn, Y.S. Jeong, I.T. Kim, S.H. Jeon, C.H. Park, Sensors 19 (2019) 1416.
[44] S. Xu, H. Zhang, Y. Wang, Corros. Eng., Sci. Technol. 54 (2019) 431–443.
[45] D. Thierry, D. Persson, G. Luckeneder, K.H. Stellnberger, Corros. Sci. 148 (2019) 338–354.
[46] Y. Zhi, D. Fu, D. Zhang, T. Yang, X. Li, Metals 9 (2019) 383.
[47] I.S. Cole, Corros. Rev. 20 (2002) 317–338.
[48] P. Roberge, R. Klassen, P. Haberecht, Mater. Des. 23 (2002) 321–330.
[49] J. Jiang, J. Wang, Yh. Lu, J.Z. Hu, Electrochim. Acta 54 (2009) 1426–1435.
[50] I.S. Cole, T. Muster, N. Azmat, M. Venkatraman, A. Cook, Electrochim. Acta 56 (2011) 1856–1865.
[51] H. Simillion, N. Van den Steen, H. Terryn, J. Deconinck, Electrochim. Acta 209 (2016) 149–158.
[52] K.Y. Law, H. Zhao, Surface Wetting: Characterization, Contact Angle, and Fundamentals, Springer, Switzerland, 2016.
[53] I.S. Cole, D. Lau, D.A. Paterson, Corros. Eng., Sci. Technol. 39 (2004) 209–218.
[54] L.R. Glicksman, A.W. Hunt, Int. J. Heat Mass Transfer 15 (1972) 2251–2269.
[55] K.R. Jensen, P. Fojan, R.L. Jensen, L. Gurevich, J. Nanosci. Nanotechnol. 14 (2014) 1859–1871.
[56] M. Singh, N.D. Pawar, S. Kondaraju, S.S. Bahga, J. Indian Inst. Sci. 99 (2019) 157–171.
[57] R. Parin, A. Penazzato, S. Bortolin, D. Del Col, Modelling of dropwise condensation on flat surfaces, in: Proceeding to the 13th International Conference on Heat Transfer, Fluid Mechanics and Thermodynamics, Slovenia, July, 2017, pp. 17–19.
[58] Y.T. Wu, C.X. Yang, X.G. Yuan, Int. J. Heat Mass Transfer 44 (2001) 4455–4464.
[59] X. Liu, P. Cheng, Int. J. Heat Mass Transfer 83 (2015) 833–841.
[60] X. Liu, P. Cheng, Int. J. Heat Mass Transfer 83 (2015) 842–849.
[61] B.S. Sikarwar, S. Khandekar, S. Agrawal, S. Kumar, K. Muralidhar, Heat Transfer Eng. 33 (2012) 301–341.
[62] P. Meakin, Phys. Scr. T44 (1992) 31–41.
[63] S. Vemuri, K. Kim, Int. J. Heat Mass Transfer 49 (2006) 649–657.
[64] E. Le Fevre, J. Rose, Int. J. Heat Mass Transfer 8 (1965) 1117–1133.
[65] R. Leach, F. Stevens, S. Langford, J. Dickinson, Langmuir 22 (2006) 8864–8872.
[66] B.S. Sikarwar, N.K. Battoo, S. Khandekar, K. Muralidhar,J. Heat Transfer 133 (2011), 021501.
[67] R. Enright, N. Miljkovic, J.L. Alvarado, K. Kim, J.W. Rose, Nanoscale Microscale Thermophys. Eng. 18 (2014) 223–250.
[68] H.J. Cho, D.J. Preston, Y. Zhu, E.N. Wang, Nat. Rev. Mater. 2 (2017) 16092.
[69] R. Wen, X. Ma, Y.C. Lee, R. Yang, Joule 2 (2018) 2307–2347.
[70] T.Q. Liu, W. Sun, C.F. Mu, S.B. Xia, X.Y. Sun, Heat Transfer-Asian Res. 42 (2013) 151–162.
[71] D. Gunasegaram, M. Venkatraman, I. Cole, Int. Mater. Rev. 59 (2014) 84–114.
[72] U.R. Evans, The Corrosion and Oxidation of Metals: Scientific Principles and Practical Applications, ACS Publications, 1960.
[73] E. McCafferty, Introduction to Corrosion Science, Springer, New York, 2010.
[74] C. Chen, F. Mansfeld, Corros. Sci. 39 (1997) 409–413.
[75] W.J. Moore, Physical Chemistry, Longman, New York, 1972.
[76] G. El-Mahdy, H.A. Al-Lohedan, Z. Issa, Int. J. Electrochem. Sci. 9 (2014) 7977–7985.
[77] T. Tsuru, A. Nishikata, J. Wang, Mater. Sci. Eng. A 198 (1995) 161–168.
[78] D. Beysens, C. R. Phys. 7 (2006) 1082–1100.
[79] S.B. Barati, N. Pionnier, J.C. Pinoli, S. Valette, Y. Gavet, Int. J. Therm. Sci. 124 (2018) 356–365.
[80] W. Xu, Z. Lan, Q. Liu, B. Du, X. Ma, Int. J. Heat Mass Transfer 127 (2018) 44–54.
[81] M.S. Venkatraman, I.S. Cole, D.R. Gunasegaram, B. Emmanuel, Mater. Sci. Forum 654-656 (2010) 1650–1653.
[82] J.S. Newman, Electrochemical Systems, Prentice-Hall, Inc., Englewood Cliffs, New Jersey, 1991.
[83] C. Marangoni, Sull'espansione delle goccie d'un liquido galleggianti sulla superfice di altro liquido, Fusi: Pavia, Italy, 1865.
[84] E. Dietrich, S. Wildeman, C.W. Visser, K. Hofhuis, E.S. Kooij, H.J. Zandvliet, D. Lohse, J. Fluid Mech. 794 (2016) 45–67.
[85] S. Somasundaram, T. Anand, S. Bakshi,Phys. Fluids 27 (11) (2015), 112105.
[86] Y.C. Chang, R. Woollam, M.E. Orazem, J. Electrochem. Soc. 161 (2014) C321–C329.
[87] Y.C. Chang, Mathematical Models for Under-deposit Corrosion in Aerated and De-aerated Solutions, Ph.D. Thesis, University of Florida, 2013.
[88] S. Li, L. Hihara, Corros. Sci. 108 (2016) 200–204.
[89] I. Cole, Materials 10 (2017) 1288.
[90] D. Sherwood, M.V. Reddy, I. Cole, B. Emmanuel, J. Electroanal. Chem. 725 (2014) 1–6.
[91] D. Sherwood, B. Emmanuel, I. Cole, J. Electrochem. Soc. 163 (2016) C675–C685.
[92] I. Cole, T. Muster, D. Lau, N. Wright, N.S. Azmat, J. Electrochem. Soc. 157 (2010) C213–C222.
[93] N. Azmat, K. Ralston, B. Muddle, I. Cole, Corros. Sci. 53 (2011) 3534–3541.
[94] I.S. Cole, R. Holgate, P. Kao, W. Ganther, Corros. Sci. 37 (1995) 455–465.
[95] S. Shevkunov, J.K. Singh, J. Mol. Liq. 264 (2018) 150–164.
[96] K.K. Varanasi, M. Hsu, N. Bhate, W. Yang, T. Deng,Appl. Phys. Lett. 95 (2009), 094101.
[97] P. Bentley, B. Hands, Proc. R. Soc. London, Ser. A 359 (1978) 319–343.
[98] L.H. Chen, C.Y. Chen, Y.L. Lee, Surf. Sci. 429 (1999) 150–160.
[99] R. Becker, W. Döring, Ann. Phys. 416 (1935) 719–752.
[100] Y.I. Frenkel, Kinetic Theory of Liquids, Dover Publication, Inc, New York, 1955.
[101] R. Sigsbee, A. Zettlemoyer, Nucleation, Marcel Dekker, Inc, New York, 1969.
[102] X.C. Zeng, J. Chem. Phys. 104 (1996) 2699–2704.
[103] M. Qian, J. Ma,J. Chem. Phys. 130 (2009), 214709.
[104] M. Qian, J. Ma, J. Cryst. Growth 355 (2012) 73–77.
[105] J. Merikanto, E. Zapadinsky, A. Lauri, H. Vehkamäki,Phys. Rev. Lett. 98 (2007), 145702.
[106] X.M. Bai, M. Li,J. Chem. Phys. 122 (2005), 224510.
[107] S. Toxvaerd, J. Chem. Phys. 119 (2003) 10764–10770.
[108] D. Niu, G. Tang, Sci. Rep. 6 (2016) 19192.
[109] K. Oh, X.C. Zeng, J. Chem. Phys. 110 (1999) 4471–4476.
[110] X. Wang, Y. Tian, X. Peng, Prog. Nat. Sci. 13 (2003) 451–456.
[111] W. Xu, Z. Lan, B. Peng, R. Wen, X. Ma, RSC Adv. 4 (2014) 31692–31699.
[112] H. Brune, Surf. Sci. Rep. 31 (1998) 125–229.
[113] J. Venables, Introduction to Surface and Thin Film Processes, Cambridge University Press, 2000.
[114] K. Oura, V. Lifshits, A. Saranin, A. Zotov, M. Katayama, Surface Science: an Introduction, Springer-Verlag, Berlin Heidelberg, 2003.
[115] J. Merikanto, H. Vehkamäki, E. Zapadinsky, J. Chem. Phys. 121 (2004) 914–924.
[116] G. Croce, E. De Candido, P. D'Agaro, Appl. Therm. Eng. 29 (2009) 1366–1374.
[117] D. Sun, J. Xu, Q. Chen, Numer. Heat Transfer, Part B 66 (2014) 326–342.
[118] S. Zheng, F. Eimann, C. Philipp, T. Fieback, U. Gross, Int. J. Heat Mass Transfer 120 (2018) 879–894.
[119] L.R. Glicksman, Int. J. Heat Mass Transfer 15 (1972) 2251–2269.
[120] C. Graham, The Limiting Heat Transfer Mechanisms of Dropwise Condensation, Ph.D. Thesis, Massachusetts Institute of Technology, 1969.
[121] E.E. Gose, A. Mucciardi, E. Baer, Int. J. Heat Mass Transfer 10 (1967) 15–22.
[122] H. Tanaka, J. Heat Transfer 97 (1975) 72–78.
[123] S. Kim, K.J. Kim,J. Heat Transfer 133 (2011), 081502.
[124] B. Qi, J. Wei, L. Zhang, H. Xu, Int. J. Heat Mass Transfer 83 (2015) 259–272.
[125] S. Khandekar, K. Muralidhar, Dropwise Condensation on Inclined Textured Surfaces, Springer, New York, 2014.
[126] M.H. Mamme, C. Köhn, J. Deconinck, J. Ustarroz, Nanoscale 10 (2018) 7194–7209.
[127] E. Dubuisson, P. Lavie, F. Dalard, J.P. Caire, S. Szunerits, Electrochem. Commun. 8 (2006) 911–915.
[128] G. El-Mahdy, A.K. Dyab, H.A. Al-Lohedan, Int. J. Electrochem. Sci. 8 (2013) 5232–5240.
[129] I. Cole, W. Ganther, D.A. Paterson, A. Bradbury, Corros. Eng., Sci. Technol. 40 (2005) 328–336.
[130] R. Picknett, R. Bexon, J. Colloid Interface Sci. 61 (2) (1977) 336–350.
[131] K. Birdi, D. Vu, A. Winter, J. Phys. Chem. 93 (1989) 3702–3703.
[132] K. Birdi, D. Vu, J. Adhes, Sci. Technol. 7 (1993) 485–493.
[133] H. Hu, R.G. Larson, J. Phys. Chem. B 106 (2002) 1334–1344.
[134] H.Y. Erbil, G. McHale, M. Newton, Langmuir 18 (2002) 2636–2641.
[135] C. Bourges-Monnier, M. Shanahan, Langmuir 11 (1995) 2820–2829.
[136] M. Shanahan, C. Bourges, Int. J. Adhes. Adhes. 14 (1994) 201–205.
[137] S. Nešić, J. Vodnik, Chem. Eng. Sci. 46 (1991) 527–537.

[138] Z. Pan, J.A. Weibel, S.V. Garimella, Langmuir 30 (2014) 9726–9730.
[139] M. Sadafi, I. Jahn, A. Stilgoe, K. Hooman, Int. J. Heat Mass Transfer 81 (2015) 1–9.
[140] C. Diddens, J.G. Kuerten, C. Van der Geld, H. Wijshoff, J. Colloid Interface Sci. 487 (2017) 426–436.
[141] C. Doursat, L. Lecoq, O. Laguerre, D. Flick, Int. J. Heat Mass Transfer 113 (2017) 1234–1245.
[142] R.G. Larson, AIChE J. 60 (2014) 1538–1571.
[143] S. Semenov, A. Trybala, R.G. Rubio, N. Kovalchuk, V. Starov, M.G. Velarde, Adv. Colloid Interface Sci. 206 (2014) 382–398.
[144] J.M. Stauber, S.K. Wilson, B.R. Duffy, K. Sefiane, J. Fluid Mech. 744 (2014) R2.
[145] K. Yang, F. Hong, P. Cheng, Int. J. Heat Mass Transfer 70 (2014) 409–420.
[146] D. Tam, V. von Arnim, G. McKinley, A. Hosoi, J. Fluid Mech. 624 (2009) 101–123.
[147] H. Hu, R.G. Larson, Langmuir 21 (2005) 3972–3980.
[148] S. Semenov, V.M. Starov, R.G. Rubio, M.G. Velarde, Langmuir 28 (2012) 15203–15211.
[149] O.E. Ruiz, W.Z. Black, J. Heat Transfer 124 (2002) 854–863.
[150] F. Girard, M. Antoni, S. Faure, A. Steinchen, Langmuir 22 (2006) 11085–11091.
[151] K. Gleason, H. Voota, S.A. Putnam, Int. J. Heat Mass Transfer 101 (2016) 418–426.
[152] Y. Chen, W. Hu, J. Wang, F. Hong, P. Cheng, Int. J. Heat Mass Transfer 108 (2017) 2072–2087.
[153] M.A. Kadhim, N. Kapur, J. Summers, H. Thompson, Langmuir 35 (2019) 6256–6266.
[154] Q. Guo, P. Cheng, Int. J. Heat Mass Transfer 134 (2019) 828–841.
[155] C. Bouchenna, M.A. Saada, S. Chikh, L. Tadrist, Interfacial Phenom. Heat Transfer 3 (2015) 185–201.
[156] S. Aksoyoglu, U. Baltensperger, A.S. Prévôt, Atmos. Chem. Phys. 16 (2016) 1895–1906.
[157] G. Meira, W. Pinto, E. Lima, C. Andrade, Constr. Build. Mater. 135 (2017) 287–296.
[158] Y.C. Chang, M.E. Orazem, ECS Trans. 50 (2013) 181–196.